Real-time study of fast-electron transport inside dense hot plasmas

A. S. Sandhu and G. Ravindra Kumar
Tata Institute of Fundamental Research, 1 Homi Bhabha Road, Mumbai 400005, India

S. Sengupta, A. Das, and P. K. Kaw
Institute for Plasma Research, Bhat, Gandhinagar 382428, India

(Received 9 February 2005; published 24 March 2006)

We offer a method to study transport of fast electrons in dense hot media. The technique relies on temporal profiling of the laser induced magnetic fields and offers a unique capability to map the hot electron currents and their neutralization (or lack of it) by the return currents in the plasma. We report direct quantitative measurements of strong electric inhibition in insulators and turbulence induced anomalous stopping of hot electrons in conductors. The present technique can prove extremely important from the point of view of fast ignition scheme, which relies on the penetration of fast electrons into the fusion core.

DOI: 10.1103/PhysRevE.73.036409 PACS number(s): 52.38.Fz, 52.65.Rr, 52.70.Ds, 52.70.Kz

Ultraintense, ultrashort lasers have given rise to the field of extreme nonlinear physics. In laser matter interactions at super-Coulombic ($>10^{16}$ W cm^{-2}) light intensities, mega-electron-volt electrons are created in large numbers, by laser photons with a millionth of that energy. Such copious fluxes of high energy electrons are of extreme importance to many areas of basic science as well as technology [1]. A promising application of such electrons is the fast ignition (FI) scheme of inertial fusion, where a beam of mega-electron-volt electrons produced at the critical layer by a petawatt scale laser is postulated to penetrate a dense, imploded fusion core and strike the fusion spark [2]. The success of this scheme not only depends on the generation of hot electrons, but also on their transport and eventual stopping in the overdense plasma. The estimation of hot electron stopping length and factors affecting it are therefore extremely important from the point of view of fast ignition physics.

The hot electron stopping length in the dense fusion plasma is affected by direct scattering and also quite significantly by anomalous mechanisms resulting from the generation of giant magnetic and electric fields. These high fields result from a combination of currents, viz. the direct hot electron current generated by the incident laser and the cold return shielding current [3] determined by the resistivity of the background plasma. If the resistivity is high, the magnitude of return current is low, creating large electrostatic fields, which exert a retarding force on the hot electrons causing anomalous stopping. If the resistivity of the background plasma is low, large return shielding currents are excited and the resulting hot and cold electron current channel is unstable to electron magnetohydrodynamic modes (sausage/kink) [4] leading to the generation of turbulent magnetic fields. This randomizes the electron motion and results in anomalous stopping of hot electrons. Both these anomalous inhibition mechanisms may contribute to the stopping of hot electrons in the fast ignition scenario. In order to estimate the stopping length, one needs to know the resistivity of the background plasma, a quantity not so well known at such extreme conditions. Based on the criterion of spark ignition it is however possible to make an estimate of the required background plasma resistivity. To ignite the spark, the core plasma with an electron density of $\sim 10^{26}$ cm^{-3} has to be heated to a temperature of 10 keV within 10 ps [5]. Following Davies [5] and using hot electron density as $\sim 10^{21}$ cm^{-3} (the critical density for 1 μ wavelength laser), the resistivity needed to satisfy the ignition criterion is approximately three orders of magnitude higher than the Spitzer resistivity at 10 keV. There already exists an indirect experimental evidence of such anomalously high resistivity [6]. Using the expression for stopping length [7], and taking stopping length as ~ 40 μ, hot electron temperature as ~ 1 MeV and $I_{\mathrm{abs}} \sim 10^{19}$ W/cm^2 [6], we get a measured estimate of resistivity which matches quite well with the required anomalous resistivity for spark ignition based on the above discussion.

It is clear that to make future progress, one needs a direct, reliable, robust, and insightful experimental method to measure the conductivity of the background plasma and the transport of hot electrons. The methods that have been used so far for monitoring the hot electron transport—while being useful—do not give this information. The most frequently adopted method for transport measurement relies on using K_α x rays from x-ray fluorophores [8,9]. In this method, hot electrons are created in a thin layer at the front of a multilayered target, travel through a layer of transport interest, and impinge on a x-ray fluorescent "screen" layer. The number of electrons at the x-ray layer is inferred from the x-ray yield. Theoretical models and estimates are then invoked to "account" for losses in the transport layer and the transport is understood based on the measurement in conjunction with the simulations. Although a worthwhile diagnostic, the x-ray fluorescence technique (XRFT) has some limitations, the most obvious being that it measures the electron number and not the "current." It does however yield an estimate of the velocity distribution of hot electrons (temperature), which is not the same as a measurement of directed hot electron "current." Also, the conductivity of the hot dense plasma which is a crucial parameter in these experiments is unknown in XRFT based measurements and has to be provided as an input in modeling the transport. Further, XRFT being a static measurement and not a "real-time" diagnostic, it does not give the most crucial information—the dynamics of hot electron transport.

Here we offer a way of monitoring this transport. We measure the temporal evolution of magnetic field—a quantity that directly depends on the fast electron and return

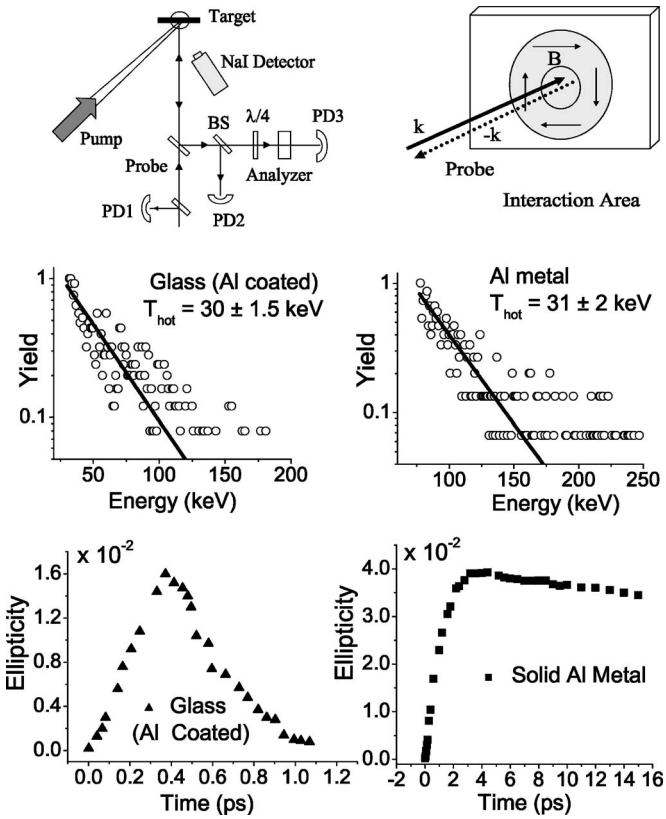

FIG. 1. Top panel: Experimental setup (PD—photo diode) and interaction region. Midpanel: Hard x-ray emission spectra for glass (coated with 0.5 μ Al) and Al metal target. Exponential fit (solid line) to deduce the hot electron temperature. Lower panel: Magnetic field induced ellipticity in glass and in Al metal target at laser intensity of 2×10^{16} W cm^{-2}.

shielding "currents" and mirrors their changes as a function of time, on ultrafast time scales. Measurement of temporal evolution of magnetic field gives an estimate of the magnetic diffusion time scale which in turn leads to an estimate of the conductivity of the background plasma (and hence of hot electron stopping length [7]) under *in situ* conditions of high temperature and pressure. In what follows, we demonstrate the method and use it to contrast the physics of hot electron transport in metals (low resistivity) and dielectrics (high resistivity). Besides giving an estimate of the background plasma conductivity and hot electron stopping length in both cases, our method gives a simple, quantitative, and direct proof of turbulent inhibition in conductors and electric inhibition in insulators. Our method is expected to be very useful for relativistic electron transport invoked in FI, as they cause colossal magnetic fields [10] and are influenced by the favorable as well as deleterious consequences of those fields.

The basic technique used here to measure the temporal evolution of magnetic field involves pump-probe experiments (Fig. 1). The laser used in these experiments produces pulses of ~100 fs duration with pulse energy of ~3 mJ. The prepulse contrast is better than 10^{-5}. The *p*-polarized pump is typically at an intensity of 2×10^{16} W cm^{-2} at 800 nm wavelength and is incident at 45°. A 10^3 weaker probe beam at second harmonic wavelength (400 nm) is incident normally. The probe laser penetrates deeper into plasma (four times higher density) than the pump and hence can sample the overdense regions, where large hot electron densities and high magnetic fields are expected to occur. The self-generated magnetic field (B) has azimuthal symmetry as hot electron jets penetrate normally into the target. The probe wave vector "**k**" is thus perpendicular to quasistatic magnetic field "**B**." In this configuration, probe traveling through magnetized plasma acquires ellipticity due to difference in refractive indices of two characteristic modes, the O wave and X wave [11]. The reflected probe is split in two parts—the first arm has a calibrated photodiode to measure reflectivity (establishes the zero of time delay), and the other has a combination of quarter wave plate and polarizer in front of photodiode to measure ellipticity. The measurement of all Stokes parameters is done with polarizer alone at 0°, 45°, 90° and then with quarter wave plate at 0° and polarizer at 45°. This yields the magnetic field induced ellipticity and rules out any presence of random depolarization in the beam [11].

As discussed earlier, we consider here two media with widely different conductivities to illustrate the two types of anomalous stopping—one a conductor (Al metal) and the other, an insulator (glass). To have an identical hot electron source in each case we use a thin coating (0.5 μm) layer of aluminum on glass sample. The hard x-ray spectrum in each case yields identical hot electron temperatures of 30 keV (±2 keV) (Fig. 1). The magnetically induced ellipticity is obtained in each case as a function of the time delay between pump and probe pulses as shown in Fig. 1. We analyze the ellipticity to obtain the magnetic field as follows. The evolution of Stokes vector (**s**) inside the magnetized plasma is determined by [11] $d\mathbf{s}/dz=\mathbf{\Omega}(z)\times\mathbf{s}(z)$. Here $\Omega=(\omega/c)(\mu_O-\mu_X)$, with μ_O and μ_X being refractive indices of O and X waves, respectively. The μ_X and hence Ω is a function of magnetic field [11]. To obtain final output Stokes vector, we integrate this equation numerically inside the plasma by dividing it into small slabs, where within each slab, the plasma parameters are assumed to be constant. For the purpose of integration, we have chosen an exponential density profile [12], though our results are rather insensitive (well within errorbars) to the exact form of the profile. Scale length of plasma is obtained, using self-similar expansion of exponential profile at ion sound speed (≈50 nm in 1 ps). The ellipticity of the reflected probe is computed from final solution $\mathbf{s_{out}}$. We find that most of the contribution to ellipticity comes from a high density region near the critical layer. This is due to the fact that, even assuming uniform magnetic field, the plasma birefringence drops by three orders of magnitude for just a factor of 20 drop in density. The two-dimensional (2D) effects due to transverse variation of intensity in our case are negligible due to high intensity and ultrashort nature of plasma excitation. We further alleviate these effects by using only the central portion of reflected beam for polarization analysis. The possible contribution to ellipticity due to refraction effects is estimated by solving Helmholtz equations and is found to be negligible as compared to observed magnetically induced ellipticity. At each time delay this scheme is implemented and the value of the magnetic field required to generate experimentally observed ellipticity is deduced. The results of the computation of the magnetic field are shown in Fig. 2 for Al and glass.

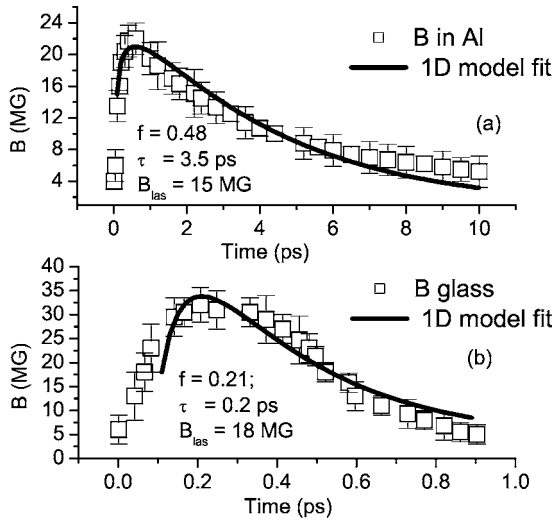

(c)

Material	Aluminum	BK7 Glass
Magnetic pulse duration	10 ps	0.9 ps
Peak Magnetic field	32 MG	22 MG
Position of peak	0.4 ps	0.2 ps
Decay constant τ	3.5 ps	0.2 ps
Conductivity σ	2.5×10^{14} s^{-1}	1.4×10^{13} s^{-1}
Penetration in 10 ps	21 μm	3 μm

FIG. 2. Magnetic field pulse profile (a) aluminum (b) glass background with laser intensity of 2×10^{16} W cm^{-2}. Solid line shows the fit obtained using hot electron modeling. (c) Comparison of transport parameters for conductor and dielectric.

From the temporal profile of magnetic field we now estimate the hot electron transport parameters *viz.* background plasma conductivity and the penetration depth of hot electrons. The temporal evolution of magnetic field is modeled as $\partial\vec{B}/\partial t=(c^2/4\pi\sigma)\nabla^2\vec{B}+(c/\sigma)(\vec{\nabla}\times\vec{j}_{\rm hot})$. This equation describes the mechanism of quasistatic magnetic field generation under EMHD approximation. Here σ is the conductivity of the background plasma as seen by the cold return shielding current and $\vec{j}_{\rm hot}=-en_h\upsilon_h$ is the current density of hot electrons, n_h and υ_h being, respectively, the density and velocity of the hot electron fluid. Under our experimental conditions, the hot electron current and the return shielding current flow in a direction normal to the target and the resultant magnetic field is in the azimuthal direction. In this geometry, the diffusion of magnetic field is assumed to be predominantly in the radial direction. This assumption is reasonably satisfied as shown later by our estimates. Using this approximation, the magnetic field evolution equation can be written as $\partial B/\partial t\approx -B/\tau+S(z,t)$ where the diffusion term is approximated as B/τ with $\tau\approx(4\pi\sigma/c^2)(\Delta r)^2$, and the source term is approximated as $S(z,t)\approx-[c/\sigma(\Delta r)]j_{\rm hot}(z,t)$. Here Δr is the laser spot radius which is about 10 μ in our experiment. Since our interest is in the estimation of σ which is related to the decay constant τ, we focus our modeling on the evolution of the magnetic field after the laser is switched off. Taking $B=B_{\rm las}$ at $t=\tau_{\rm laser}$, the solution of the above equation is given by $B\approx B_{\rm las}e^{-(t-\tau_{\rm laser})/\tau}-e^{-t/\tau}\int_{\tau_{\rm laser}}^{t}(c/\sigma\Delta r)j_{\rm hot}(z,t)e^{t/\tau}dt$ where we have substituted the expression for $S(z,t)$. To make an estimate of $j_{\rm hot}$ (i.e., n_h and υ_h), we use the formalism given by Bell *et al.* [7], where the evolution of hot electron density (n_h) is governed by a nonlinear diffusion equation of the form $\partial n_h/\partial t=(\partial/\partial z)[(\sigma T_h/e^2n_h)(\partial n_h/\partial z)]$, T_h being the hot electron temperature. Since our interest lies in $t>\tau_{\rm laser}$, we use the self-similar solution of the nonlinear diffusion equation in this temporal regime, as $n_h=(2n_0z_0/\pi)[L/(z^2+L^2)]$ with $L(t)=z_0[(5\pi\sigma T_h/3e^2n_0z_0^2)(t-\tau_{\rm laser})+1]^{3/5}$ where $n_0=(2/9)(I_{\rm abs}^2\tau_{\rm laser}e^2/\sigma T_h^3)$ and $z_0=(3\sigma T_h^2/e^2I_{\rm abs})$ [7]. Here n_0 is the density of hot electrons at $z=0$ (the critical point of the pump beam), at time $t=\tau_{\rm laser}$ and z_0 is the characteristic stopping length such that n_0z_0 is the total number of hot electrons produced at time $t=\tau_{\rm laser}$. Both n_0 and z_0 depend on the absorbed intensity $I_{\rm abs}=fI_{\rm incident}$, f being the fraction absorbed. Using the expression for n_h and $L(t)$, we now estimate $j_{\rm hot}$ as $j_{\rm hot}=-en_h\upsilon_h=-e(2n_0z_0/\pi)(L/z^2+L^2)[\alpha(dL/dt)]$ where υ_h, the hot electron velocity is taken to be proportional to dL/dt, α being the proportionality constant. Substituting the expression for dL/dt in $j_{\rm hot}$ and using $\sigma=[c^2/4\pi(\Delta r)^2]\tau$, we get the following final expression for the magnetic field:

$$B=B_{\rm las}e^{-y}+Ae^{-y}\tau\int_0^y\frac{(py\tau+1)^{1/5}e^y}{z^2+z_0^2(py\tau+1)^{6/5}}dy, \qquad (1)$$

where $y=(t-\tau_{\rm laser})/\tau$, $A=2cz_0\alpha T_h/e\Delta r$, and $p=5\pi\sigma T_h/3e^2n_0z_0^2$. We use the above expression for $B(t,z)$ at $z=0$ (pump critical density) to model the magnetic field evolution as a function of time using τ (which is related to conductivity σ) and f as free parameters. The proportionality constant α is taken to be unity. The magnetic field at time $t=\tau_{\rm laser}$ i.e., $B_{\rm las}$ is 15 and 18 MG, respectively for aluminum and glass. The best fit curves (solid lines) are shown in Figs. 2(a) and 2(b), respectively. From the best fit, the relevant parameters (f and τ) for aluminum and glass are aluminum: $f=0.48$; $\tau=3.5$ ps and glass: $f=0.21$; $\tau=0.2$ ps.

The data and the fits in Fig. 2 show that the time for magnetic field decay in aluminum is an order of magnitude larger than in glass. We compare the two cases to extract the conductivity $\sigma=[c^2/4\pi(\Delta r)^2]\tau$ from the decay time constant τ (representing magnetic diffusion time scale). The τ values from fits in Fig. 2 yield conductivities for two cases differing by more than an order of magnitude viz. $\sigma_{\rm Al}=2.5\times10^{14}$ s^{-1} and $\sigma_{\rm glass}=1.4\times10^{13}$ s^{-1}. We note here that the conductivities thus deduced are "effective conductivities" which do not depend on any specific microscopic model. We further note that the conductivity of glass as deduced above is not affected by the presence of aluminum coating because of its negligible expansion in a picosecond. In the case of glass, which is almost nonconducting ($\sigma\sim0$) at low temperatures, the actual dynamics of finite return current formation is complex. One can attribute this finite conductivity at elevated temperatures to target heating by collisional effects and ionization via large electric fields exceeding breakdown threshold. Similarly, the normal conductivity of Al is known to be $\sigma\sim3.5\times10^{15}$ s^{-1} and it is expected to reduce due to turbulence effects [13,14]. Thus the results here are estimates of the nonzero finite conductivity of glass and turbulent conductivity of Al. Moreover, the electrostatic effects in glass are found to be an order of magnitude stronger than the turbulent mechanisms in aluminum in inhibition of electron

transport. We now estimate the penetration depth L_f of hot electrons in the time regime of interest using the expression for $L(t)$. Using the parameters z_0 and σ from the 1D model fitting and T_{hot} from observations, we get for glass, $L_f=7.3\times10^{-5}$ cm in 1 ps and 3.0×10^{-4} cm in 10 ps, and for aluminum $L_f=2.1\times10^{-3}$ cm in 10 ps. Our estimate of penetration depth for aluminum justifies our assumption of predominance of radial diffusion of magnetic fields. In the case of glass, the assumption does get violated, but it is to be noted here that ours is the first work which gives at least an order of magnitude estimate of glass resistivity at $\sim$100 eV. The results thus indicate that hot electrons are penetrating an order of magnitude more distance in a conducting background for a given time duration. In summary, Fig. 2(c) shows the comparison between Al and glass.

We have obtained here quantitative estimates of background plasma conductivity and penetration depth of hot electrons in glass and aluminum. Further these results are probably the first evidence of the role of turbulent inhibition in a conductor (Al) vis a vis electric inhibition in a dielectric (glass). The electric inhibition has been qualitatively observed earlier in plastic targets using K_α emission from XRFT [8,9]. However as pointed our earlier, XRFT has its limitations and now we offer further comparison of this technique with the magnetic field technique. The magnetic field technique described here is based on certain assumptions about scale length, density profile, and uniform electrical conductivity. These assumptions have been justified to some extent and further refinements of this method can yield more accurate results. However, even in the presence of these limitations, the magnetic field method has distinct advantages over XRFT measurements. XRFT measurements are typically done only at a few discrete thicknesses, which lead to considerable uncertainties in deduced hot electron ranges. Unlike in XRFT, low as well as high electron fluxes can be monitored in magnetic field measurements. The limiting value was about 1 MG in our case when "noise" ellipticity due to refraction effects becomes significant. This corresponds to currents as low as 10 kA. With present configuration we can measure currents as high as 2 MA. It is easy to envision that this technique can probe up to solid density using higher (fifth or seventh) harmonic of IR laser, allowing us to probe deeper into plasma and also measure higher magnetic fields and currents. In the magnetic field technique, a concrete macroscopic fluid model yields direct evidence of noncollisional transport mechanisms and also gives quantitative estimates of the transport coefficients (viz. background conductivity). X-ray technique requires background conductivity as an uncertain input to model noncollisional effects. Unlike in XRFT, we can estimate heating of plasma $J^2/\sigma_{\mathrm{eff}}$ as we measure current directly. In x-ray technique, certain energy flux and distribution of electrons is estimated at the source and losses are postulated and simulated using collisional Monte Carlo codes. Thus the final flux incident at fluorescent layers is then compared with these calculations and any deviation from the simulation result is interpreted as evidence of inhibition. In an insightful paper [15], Davies has shown that collisional Monte Carlo simulations can be significantly in error in estimating transport.

In conclusion, we propose a measurement of hot electron transport in dense hot media via magnetic field profiling, i.e., studying the temporal evolution of self-generated magnetic field via pump-probe polarimetry. We obtain quantitative estimates of electric field related inhibition of the transport in dielectric media and turbulence effects dominated inhibition in conductors. Our results on magnetic pulse measurement and modeling in terms of hot electron currents yield measurements of "effective" transport coefficients of conducting and dielectric media under extreme conditions. We understand that in reality, this effective conductivity will in general be a function of space and time; but this being the subject of our future investigation will be reported later. The present results and techniques are very important for laser fusion schemes, which rely on the ignition of hot spot by energy deposition by fast electrons.

One of us (S.S.) would like to thank J. R. Davies for useful discussions.

[1] P. Gibbon and E. Forster, Plasma Phys. Controlled Fusion **38**, 769 (1996).
[2] R. Kodama *et al.*, Nature (London) **418**, 933 (2002).
[3] Y. Sentoku*et al.*, Phys. Rev. E **65**, 046408 (2002); Y. Sentoku *et al.*, Phys. Plasmas **6**, 2855 (1999).
[4] A. Das and P. K. Kaw, Phys. Plasmas **8**, 4518 (2001); N. Jain *et al.*, *ibid.* **10**, 29 (2003); N. Jain, A. Das, and P. K. Kaw, *ibid.* **11**, 4390 (2004).
[5] J. R. Davies, Phys. Rev. E **68**, 056404 (2003).
[6] R. Kodama *et al.*, Nature (London) **412**, 798 (2001).
[7] A. R. Bell, Plasma Phys. Controlled Fusion **39**, 653 (1997); A. R. Bell, J. R. Davies, and S. M. Guerin, Phys. Rev. E **58**, 2471 (1998).
[8] D. J. Bond, J. D. Hares, and J. D. Kilkenny, Phys. Rev. Lett. **45**, 252 (1980); D. J. Bond *et al.*, Plasma Phys. Controlled Nucl. Fusion Res. **24**, 91 (1982).
[9] F. Pisani *et al.*, Phys. Rev. E **62**, R5927 (2000); K. Wharton*et al.*, Phys. Rev. Lett. **81**, 822 (1998); L. Gremillet *et al.*, *ibid.* **83**, 5015 (1999).
[10] U. Wagner *et al.*, Phys. Rev. E **70**, 026401 (2004).
[11] E. Collet, *Polarized Light* (Marcel Dekker, New York, 1993); S. E. Segre, Plasma Phys. Controlled Fusion **41**, R57 (1999).
[12] W. L. Kruer, *The Physics of Laser Plasma Interactions* (Addison-Wesley, New York 1988); P. Mora, Phys. Rev. Lett. **90**, 185002 (2003).
[13] J. F. Drake, R. G. Kleva, and M. E. Mandt, Phys. Rev. Lett. **73**, 1251 (1994); A. Das and P. H. Diamond, Phys. Plasmas **7**, 170 (2000).
[14] Y. Sentoku, K. Mima, P. Kaw, and K. Nishikawa, Phys. Rev. Lett. **90**, 155001 (2003).
[15] J. R. Davies, Phys. Rev. E **65**, 026407 (2002).